PNAS
www.pnas.org

Supplementary Information for

A multi-million-year-old record of Greenland vegetation and glacial history preserved in sediment beneath 1.4 km of ice at Camp Century

Andrew J. Christ*[a,b], Paul R. Bierman[a,b,c], Joerg M. Schaefer[d], Dorthe Dahl-Jensen[e,f], Jørgen P. Steffensen[e], Lee B. Corbett[a], Dorothy M. Peteet[d,g], Elizabeth K. Thomas[h], Eric J. Steig[i], Tammy M. Rittenour[j], Jean-Louis Tison[k], Pierre-Henri Blard[k,l], Nicolas Perdrial[a], David P. Dethier[m], Andrea Lini[a], Alan J. Hidy[n], Marc W. Caffee[o,p], John Southon[q]

* Correspondence to Andrew Christ
Email: andrew.christ@uvm.edu

This PDF file includes:

Supplementary Information Text

Detailed sedimentological description

The entire basal sediment section is 3.44 m thick (~0.1 m in diameter). It is divided into three units: i) an upper diamicton unit (1.18 m thickness, average density: 2.0 g cm^{-3}, weak red [2.5YR 4/2]), which is more sand-rich near the top and contains sub-angular to sub-rounded granules and pebbles in an unsorted sandy matrix downcore. ii) A debris-rich ice layer (0.89 m thickness, average density: 1.0 g cm^{-3}). The contact between the upper diamicton and the debris-rich ice layer is rough and non-horizontal, suggesting erosion or deformation during emplacement of the upper diamicton. The intermediate debris-rich ice layers include superimposed sub-vertical and oblique clean ice lenses. iii) A lower diamicton unit (1.37 m thickness, average density: 2.1 g cm^{-3} ; reddish gray [5YR 5/2]) with unsorted sub-angular to sub-rounded pebbles (up to 8 cm) supported by an non-stratified clay-rich sand matrix. The lower diamict also contains sub-horizontal ice lenses. In both upper and lower diamictons, pebble, granule, and coarse sand grains are characterized by heterogenous lithologies. Combining our observations with those of (1), we identified at least 6 different rock types in these two units: granites, tonalites, granodiorites, metagabbros, sandstones and metasediments. Such a large variety of rock types is unlikely to be observed in colluvium or scree diamicton, that is by definition local and generally only contains one or two rock types. Instead, the lithological heterogeneity more likely reflects the mixing of variable rock sources eroded over a large (>100 km^2) basin. Moreover, our macroscopic and microscopic observations revealed abrasion marks on the sand and pebble grains. Both of these characteristics are typical of glacial processes. Binocular microscopic observation of the coarse sand fraction processed for in situ ^{10}Be and ^{26}Al indicates that quartz grains were predominantly sub-rounded to rounded with some sub-angular grain edges.

Burial age calculations

Cosmogenic radionuclides with different mean-lives (τ), such as ^{26}Al (τ_{26} = 1.01 Myr (2)) and ^{10}Be (τ_{10}= 2.02 Myr (3, 4)), can be used to determine the duration of burial since Earth materials were exposed at the surface (5). In constantly exposed or steadily eroding landscapes, ^{26}Al and ^{10}Be accumulate in quartz mineral lattices through interaction with cosmic rays at known rates, and thus at a predictable ratio. In Greenland, ^{26}Al and ^{10}Be are thought to be produced at a ratio ($^{26}Al/^{10}Be$) of 7.3±0.3 (6), although this ratio is lower elsewhere (nominal global value: 6.75 (7)). Once materials are buried at depths where nuclide production is much lower, $^{26}Al/^{10}Be$ decreases as burial time increases. Given the measured ^{10}Be and ^{26}Al concentrations, the production ratio and thus burial age calculations, are negligibly affected by changes in elevation.

We calculated simple burial ages using the ^{26}Al and ^{10}Be measurements from the upper sample (1059-4; n=6) and lower sample (1063-7, n=3). Such burial ages can only be interpreted as absolute ages of sediment emplacement if the buried materials: (i) were constantly exposed or steadily eroding prior to eroding, and do not have a previous complex burial history; and (ii) did not experience post-burial nuclide production either through re-exposure or shallow burial (8). The Camp Century subglacial sediments do not satisfy these restrictive assumptions, and therefore simple burial ages constrain only a maximum duration of burial since the time of last exposure.

Based on the measured $^{26}Al/^{10}Be$ ratios, we calculate cosmogenic minimum total histories (exposure plus burial), which provide a maximum age for the most recent ice-free exposure, not necessarily the timing of deposition or a single, finite burial age (9). Cosmogenic $^{26}Al/^{10}Be$ minimum total histories were modelled using MATLAB® code from (9, 10) using the world-average production rate and scaling implemented in the CREp calculator (11). We assumed that exposure occurred at the present bedrock elevation at Camp Century (500 m above sea level). We do not use the isostatic uplift-corrected elevation for these measured ^{10}Be and ^{26}Al concentrations because the $^{26}Al/^{10}Be$ ratio and burial age calculations are unaffected by elevation change (10). We assume no significant muon production of cosmogenic ^{10}Be or ^{26}Al

because the sediment has been buried below thick (>1000 m) glacial ice for a prolonged period of time (12). We modified the code from default values to use a surface production $^{26}Al/^{10}Be$ ratio of 7.3 (6), which is higher than what was originally applied to calculations constraining the exposure and burial history of the GISP2 bedrock core ($^{26}Al/^{10}Be$ = 6.75) (13). We report weighted average $^{26}Al/^{10}Be$ ratios and simple burial ages using the inverse of the square root of the 1σ uncertainty for the $^{26}Al/^{10}Be$ of individual samples as weighting factors.

Luminescence measurements

Luminescence dating provides an age estimate of the time since sediment was last exposed to light, which resets the luminescence signal (14). The presence of abundant and well-preserved terrestrial plant material indicates that the sediments represent a former land surface and are good candidates for luminescence dating. Samples were received at the Utah State University (USU) Luminescence lab in their original frozen state to keep the sediment intact and reduce light exposure to the inner portion of the sediment chips. Samples were given unique lab numbers (1059-4: USU-3195, 1063-7: USU-3196) and processed under dim amber safe-light (~590 nm) in a darkroom. The outer portions of each sediment chip were previously exposed to light during storage and further exposed to light during sub-sampling. To remove the light-exposed sediment, the outer 2 mm of each sample was shaved off using a razor blade while the sediment was kept frozen using a block of dry ice. Only a small portion of inner sediment was available for dating due to small sample sizes, limiting the number of replicate analyses (n<20 per sample).

The innermost sediment in each sample was sieved to separate the 150-350 μm fraction, treated with 10% HCl and 3% H_2O_2 to remove carbonates and organics, and floated in 2.72 g/cm^3 and 2.58 g/cm^3 sodium polytungstate to isolate the quartz and potassium feldspar fraction. Due to the small amount of sediment, the quartz fraction was not treated with HF and the limited number of tests of the quartz luminescence signals followed the post-IR blue stimulation method (15). Initial tests of 1059-4 (USU-3195, upper-most sample) produced little natural luminescence signal in the quartz and feldspar fractions, indicating too much light exposure during storage and subsampling. The original position of each sediment chip in the larger core sections is not known and it could be that the chip from 1059-4 sub-sampled for luminescence dating was collected from the outer portions of the stored sediment and may have received considerable light exposure prior to arrival at the USU Luminescence Lab. Measurements of the quartz fraction of 1063-7 (USU-3196, lowermost sample) indicated that the natural signal is in saturation, and thus beyond dating range with quartz OSL. All-remaining measurements were conducted on the feldspar fractions of 1063-7.

Luminescence was measured using a Risø TL/OSL Model DA-20 reader using IR emitting diodes (875 nm) as the stimulation source and signal detection through a combination of Schott BG-39 and Corning 7-59 filters (320-450 nm). IRSL measurements followed the single-aliquot regenerative-dose method for feldspars (16) using two techniques that reduce anomalous fading effects (loss of signal with time), which is common with feldspars. The measurements followed the high temperature post-infrared IRSL (p-$IRSL_{225}$,(17, 18)) method with IR stimulation at 225 ºC for 100 s following IR stimulation at 50 ºC for 100 s and included fading correction (14, 19). The second set of measurements utilized a modified pIRSL protocol with multiple elevated temperatures (MET-pIRSL (20). An equivalent dose (De) value is calculated from IR stimulated luminescence signal at progressively higher temperatures (50-300 ºC, at 50 ºC temperature steps, each measured over 100 s). The De values used for age determination were calculated from the central age model (21) of the 200 ºC and 250 ºC MET-pIRSL measurement steps.

Luminescence ages are calculated by dividing the equivalent dose of radiation the sample received during burial (De, in Grays where 1 Gy = 1 Joule kg^{-1}) by the radioactivity of the surrounding sediment (dose rate, in Gy kyr^{-1}). Dose rate values for each sample were determined using ICP-MS and ICP-AES on sub-samples from each core segment (Table S9). Elemental concentrations were converted to dose rate using conversion factors (22) and corrected for beta-

dose attenuation due to grain-size (150-350 μm) (23) and water content (20%) (24). Due to internal K in the feldspar grain, dose rates include contribution from internal alpha dose (25) and its attenuation (a-value = 0.089 ± 0.01) (26). The samples are assumed to have no cosmic ray contribution to the dose rate due to burial by the 1390 m of overlying ice, following equations of (27). Moisture content used for dose-rate attenuation correction was measured on both samples as the difference in mass between their initial frozen state and following 24 hours in a drying oven. Dose-rate uncertainties were calculated in quadrature using the methods of (28–30) and include uncertainty in the elemental concentrations related to ICP detection limits (31), 30% uncertainty in moisture content and 3% uncertainty for dose-rate conversion (32).

Results from both IRSL measurement techniques are presented in Table S10 and De distributions are presented in Figure S3. Dose response measurements indicate that the natural luminescence signals were near or beyond saturation and results should be considered minimum age estimates. Saturation doses (2*Do) ranged from 1140 ±620 Gy for the $pIRSL_{225}$ measurements and 2220 ±520 Gy for the MET-$pIRSL_{200,250}$ measurements (200 and 250 °C temperature steps), indicating that more reliable older ages can be obtained from the MET-pIRSL technique. This is expected as the higher heat treatments should sample luminescence traps that are less prone to fading and may have higher saturation levels (20). The fading corrected p-$IRSL_{225}$ results suggest the basal sample was last exposed to light at least 0.7 Myr and the MET p-$IRSL_{200, 250}$ results suggest the sample was deposited prior to 1.4 Ma.

Paleo-elevation and temperature calculations

Removal of the Greenland Ice Sheet would cause isostatic uplift of bedrock at the site. Most of the uplift would occur in 10 kyr, the average duration of an interglacial. At present ice thickness at Camp Century is 1382 m. Assuming ice (ρ_{ice}) and bedrock (ρ_{rock}) densities of 917 kg/m^3 and 2800 kg/m^3, respectively, and converting the firn layer to ice-equivalent thickness (H_{ice} = 1382 – 25 m), the equilibrium uplift h_{uplift} is $H_{ice}(\rho_{ice}/\rho_{rock})$ = 444 m. Removal of the ice sheet (-1382 m) and subsequent glacial isostatic adjustment (+444 m) would result in a net surface elevation change of -952 m at Camp Century.

We estimate the impact of 952 m of surface lowering on the water-isotope values assuming a $\delta^{18}O$/altitude effect of 0.6 ‰/100 m (33). A net decrease of 952 m from the present ice surface elevation would constitute (0.6 ‰/100 m) * 952 m = 5.7 ‰ of $\delta^{18}O$ enrichment. The pore-ice $\delta^{18}O$ values (Table S2) are 5.9 ‰ to 7.5 ‰ greater than modern precipitation (–29‰) at Camp Century. This implies that between 0.2 ‰ and 1.8 ‰ enrichment is unexplained by -952 m of elevation change. Converting these values to temperature change using $\partial(\delta^{18}O)/\partial T$ = 0.7 ± 0.1 ‰/°C yields 0.3 ± 0.1 °C and 2.6 ± 0.4 °C. Note that these values account for the uncertainty in the $\delta^{18}O$/T sensitivities, but not in total elevation change, which is provided only as an example; accounting for elevation change uncertainty requires greater knowledge of the timing and extent of deglaciation than is available. Small changes in $\delta^{18}O$ could also have resulted from melting-refreezing processes within the permafrost sediment, but any significant shift would be likely be accompanied by anomalous deuterium excess values, which we do not observe.

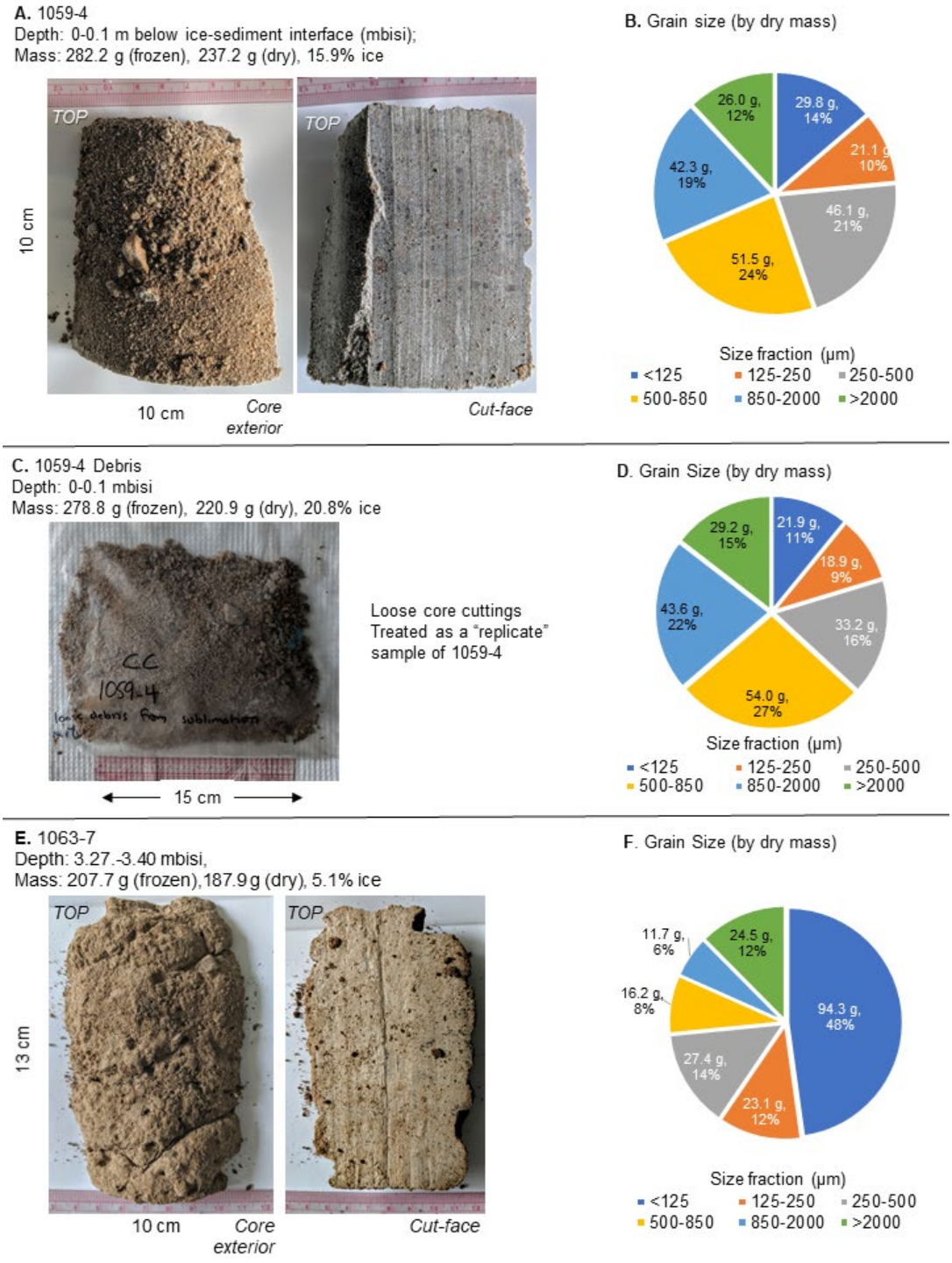

Fig. S1. Core sample information, photos, and grain size distributions of basal material samples (A&B) 1059-4, (C&D) 1059-4Debris, and (E&F) 1063-7. Note: the grain size fractions presented were operational size fractions for lab work.

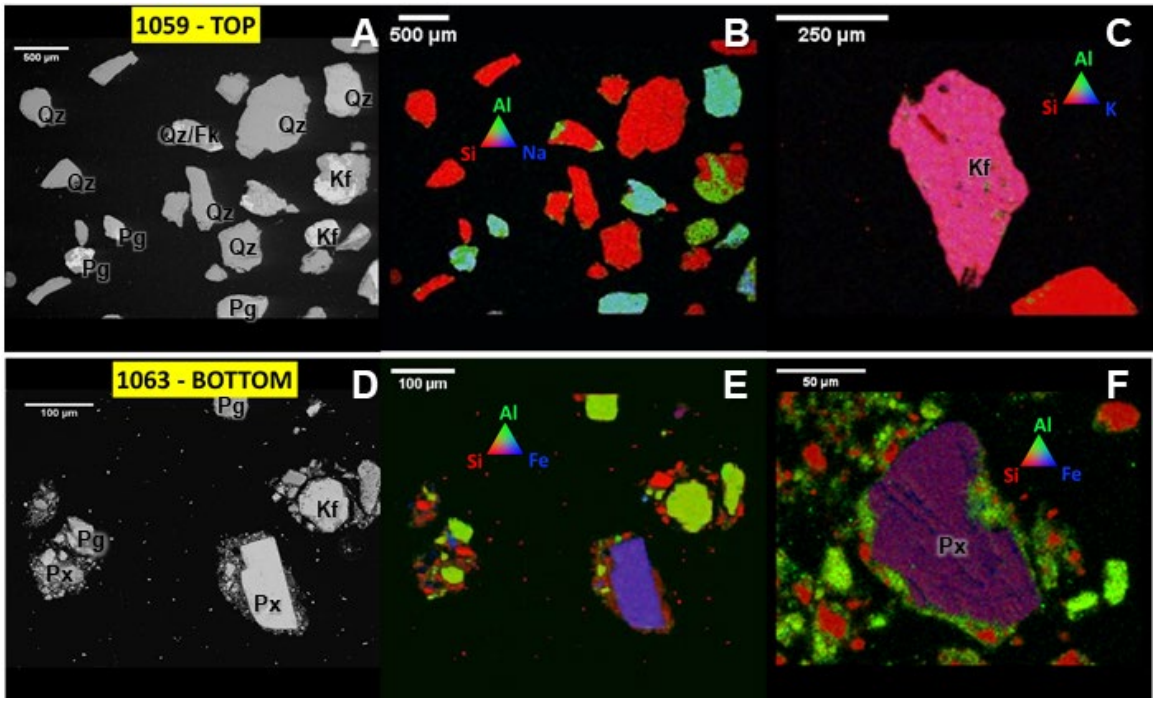

Fig. S2. SEM/EDS analyses of grain coatings. (A-C) SEM/EDS images and analyses for 1059-4 (Q: quartz, Kf: potassium feldspar, Pg: plagioclase) showing A) SEM image and chemical maps of Si, Al and Na (B) and Si, Al, and K (C). (F-H) SEM/EDS images and analyses of 1063-7 (Pg: plagioclase, Px: pyroxene) showing F) grain SEM image and chemical maps of Si, Al, and Fe (G-H).

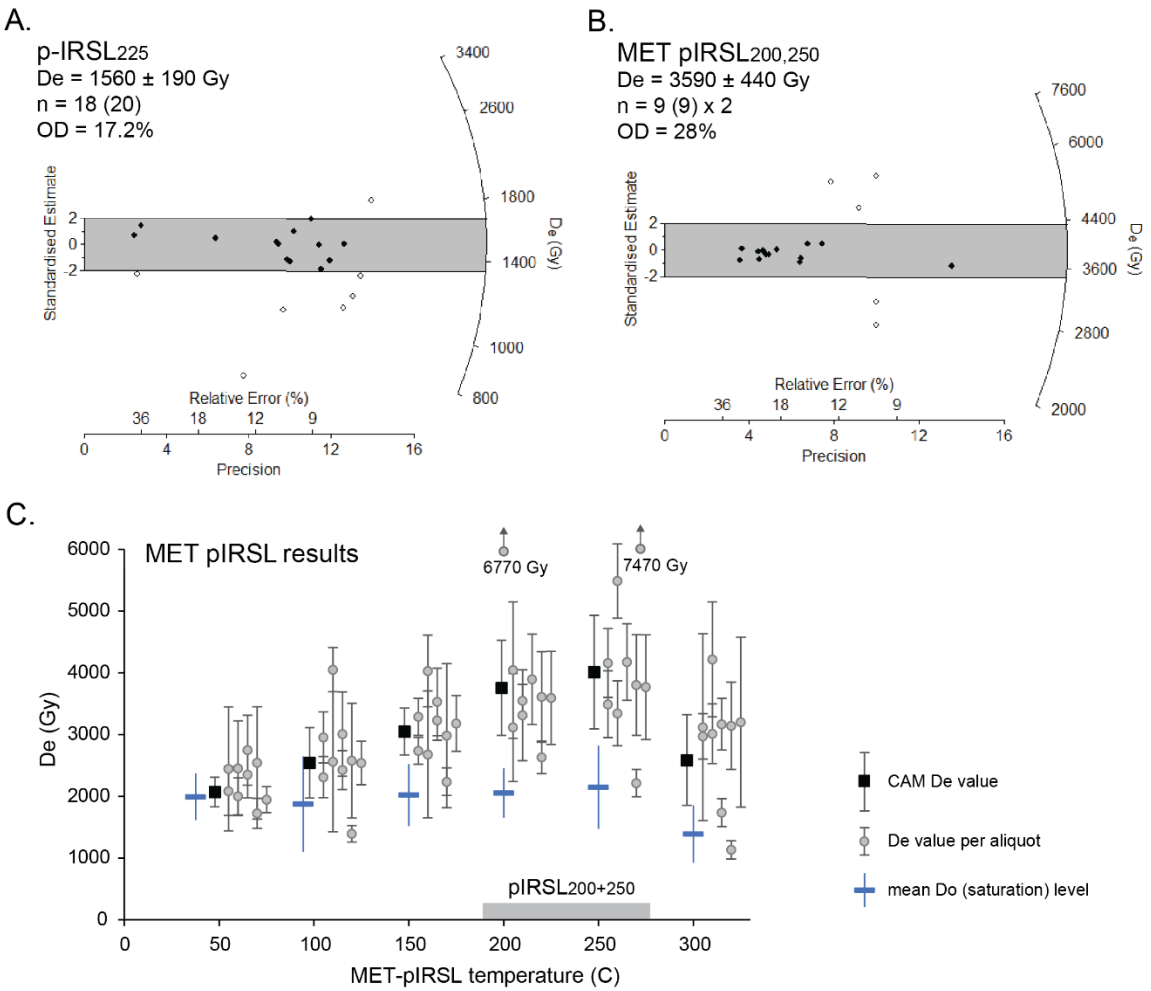

Fig. S3. Luminescence results for sample 1063-7, lower diamicton. (A) Radial plot displaying the equivalent dose (De) distribution results from the post-infrared stimulated luminescence at 225°C ($p\text{-IRSL}_{225}$). (B) Radial plot showing the De distribution results from the 200°C and 250°C steps from the multiple elevated temperature p-IRSL analyses (MET-pIRSL) of the same sample. (C) Results of all temperature steps from the MET-pIRSL analyses. De results from the 200°C and 250°C p-IRSL temperature steps form a general plateau in IRSL ages. This plateau was interpreted to represent the most stable electron traps that were less affected by anomalous fading (loss of signal over time). The mean Do (saturation levels) of each group of aliquots are plotted to show that most aliquots are saturated and therefore cannot determine an absolute age. Instead all results reported here should be interpreted as minimum age estimates.

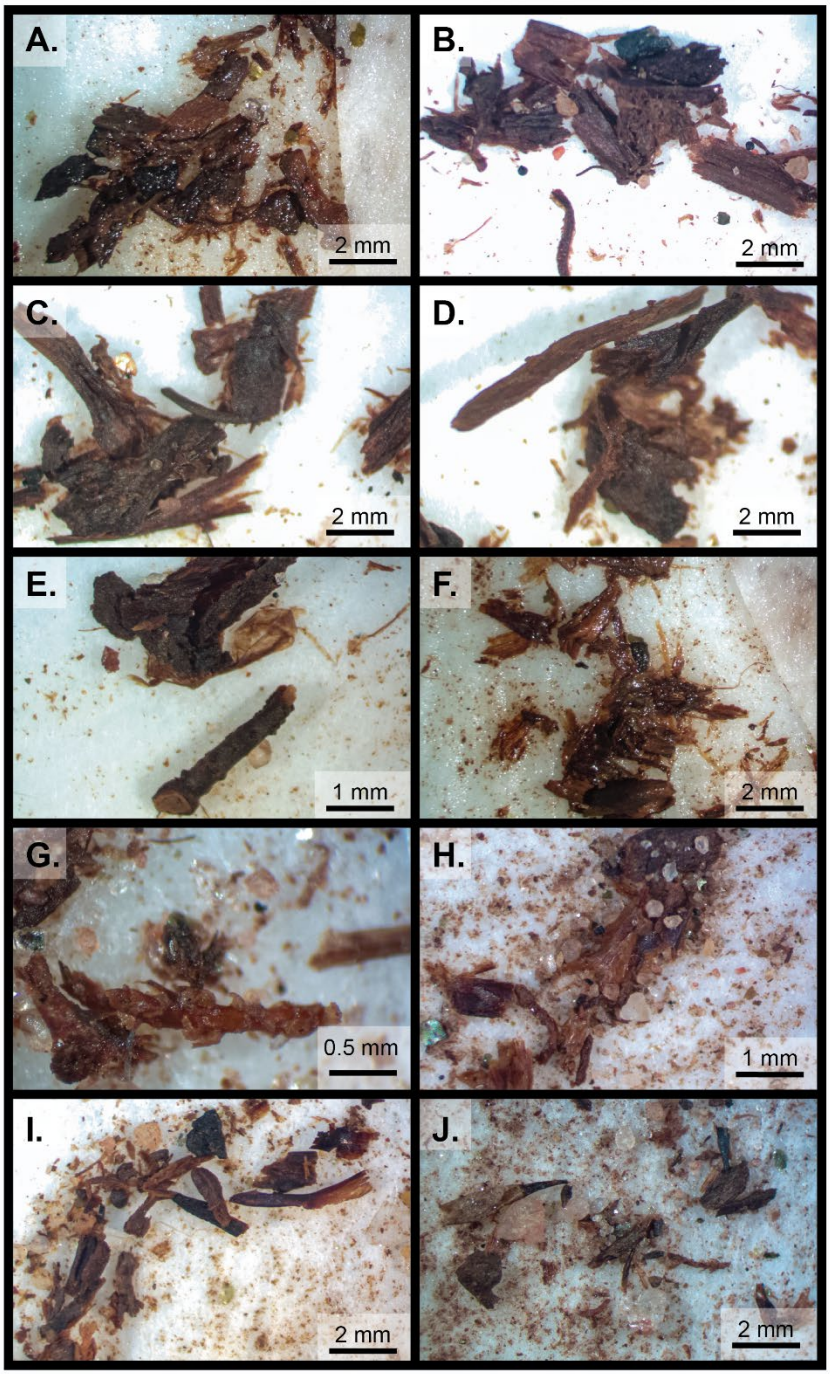

Fig. S4. Micrographs showing macrofossils recovered from 1059-4 that includes (A-J) woody debris and twigs (D, E), bryophyte stems (G).

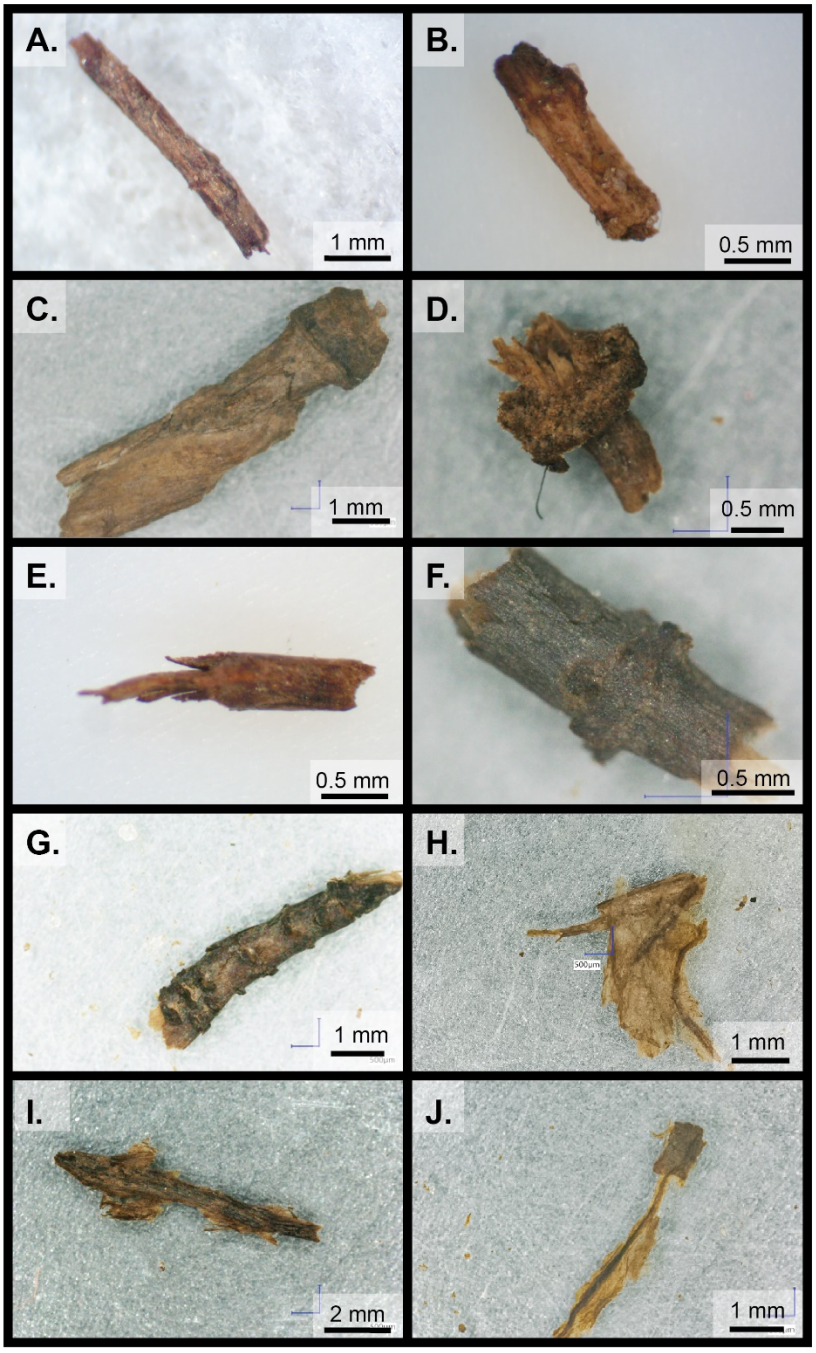

Fig. S5. Micrographs showing macrofossils recovered from 1059-4 that includes twigs and stems (A-E), possible *Empetrum* twigs (F,G), and possible sedge fragments (H-J).

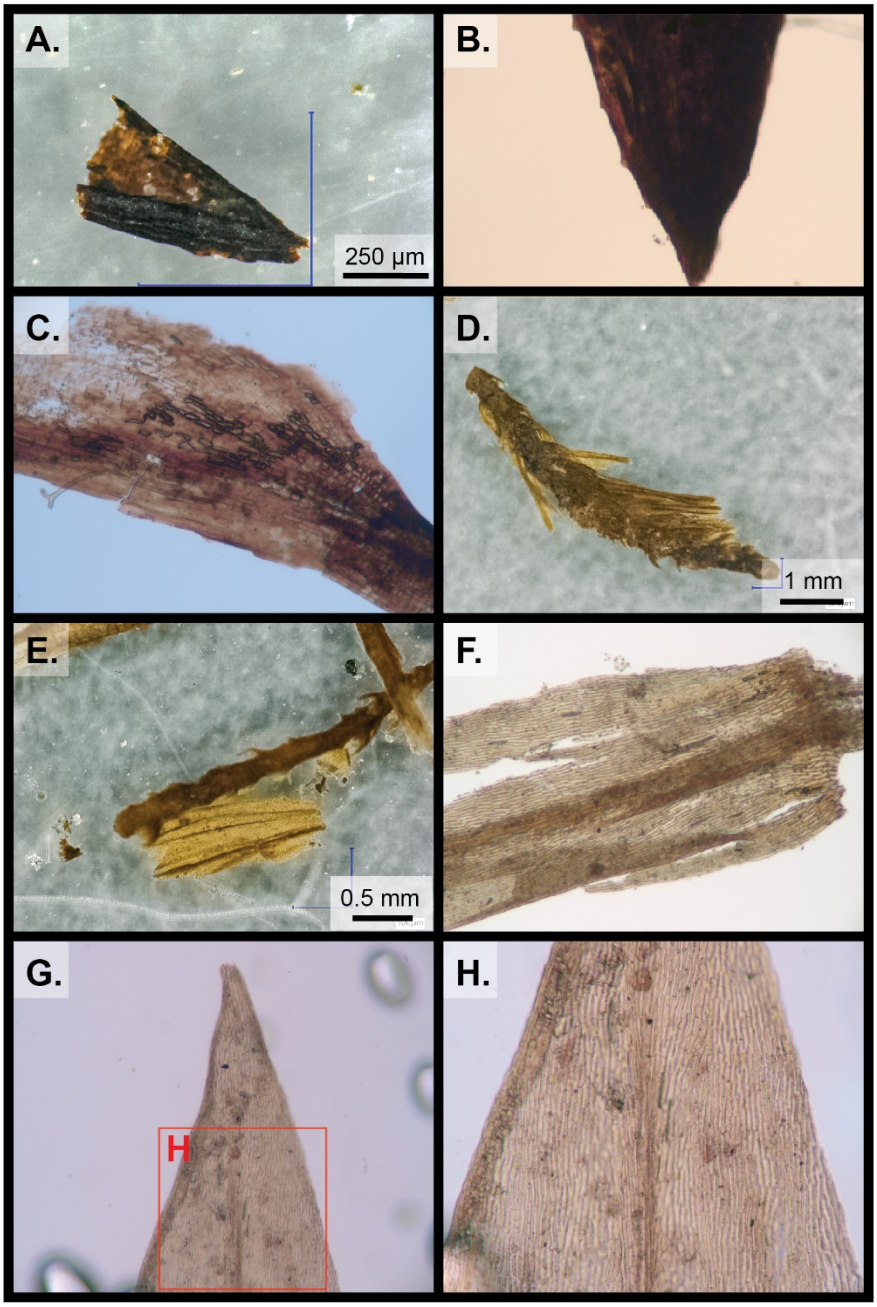

Fig. S6. Micrographs of macrofossils recovered from 1059-4 including *Polytrichum juniperinum* leaf tips (A,B) and cells (C), *Tomentypnum nitens* plicate leaves (D, E) , alar cells (F), and upper leaf cell structure (G-H). Magnification is 100x on B,C, F and G, and 250x on H.

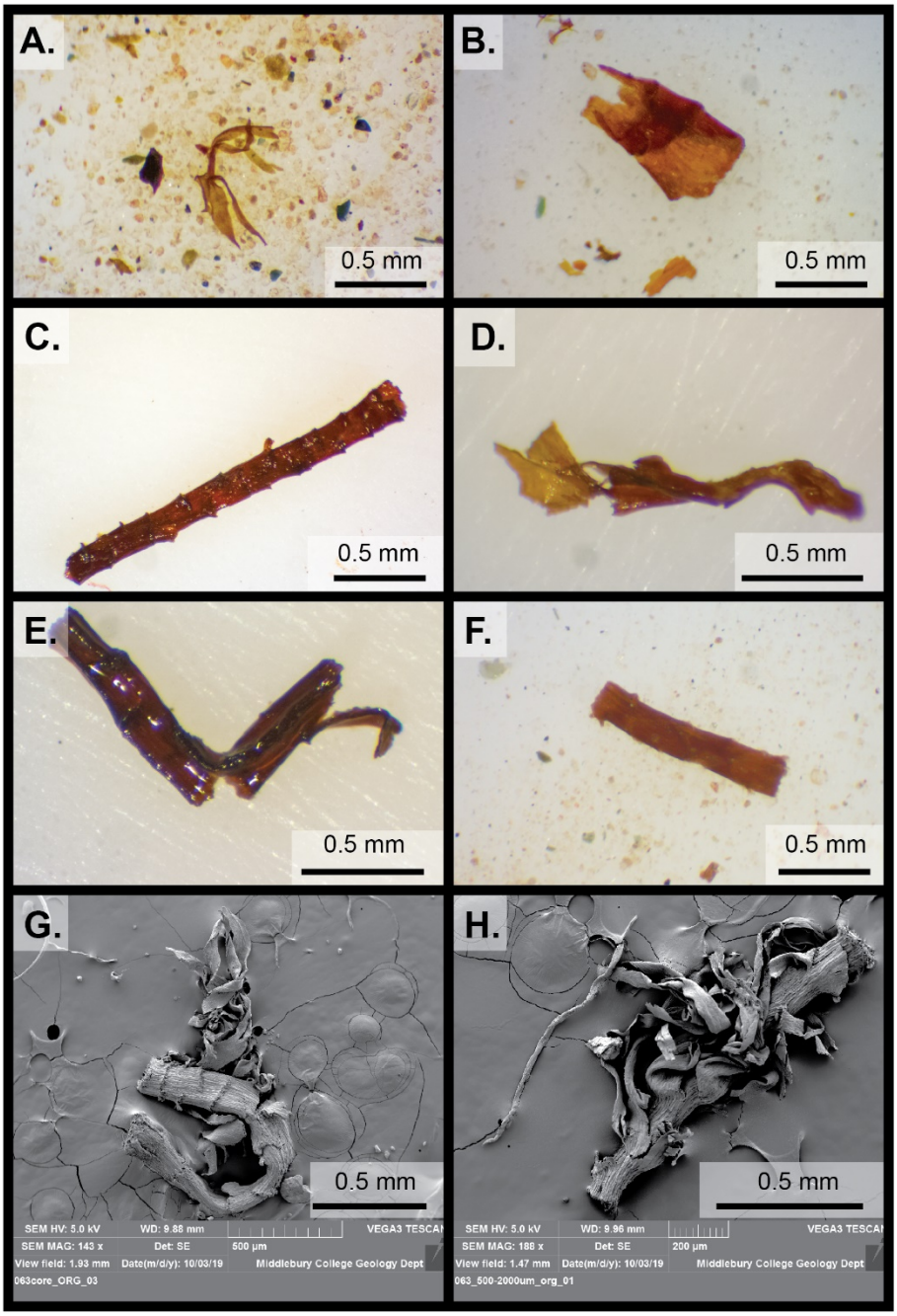

Fig. S7. Macrofossils recovered from 1063-7 including bryophyte leaf (A) and stem fragments (B-F). SEM images of bryophyte stems with leaves (G,H). Note macrofossils in 1063-7 were not as well preserved as 1059-4, and generally consisted of smaller plant fragments.

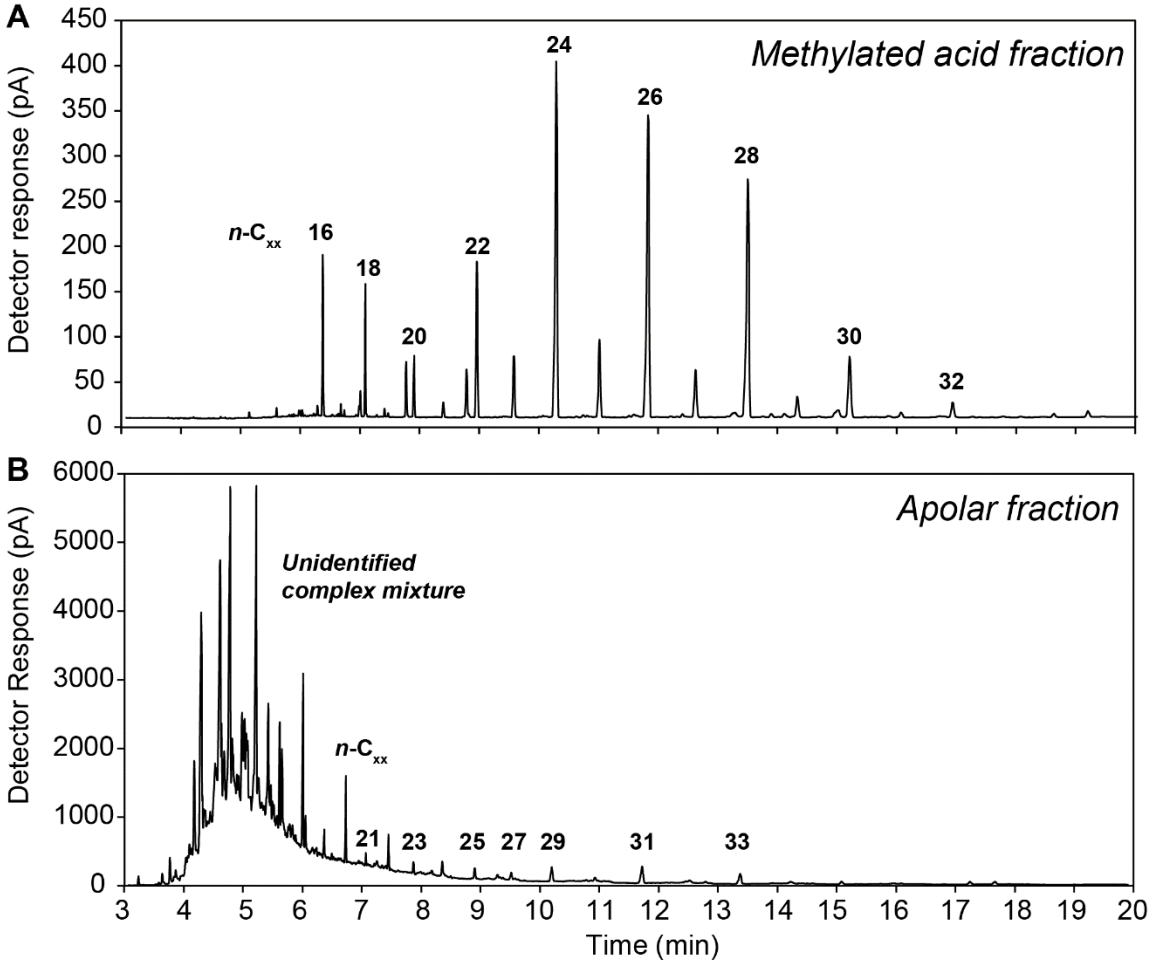

Fig. S8. Biomarker chromatogram for 1063-7 (A) methylated acid fraction (*n*-alkanoic acids), even chain length fatty acid methyl ester peaks labeled with carbon chain number. (B) Apolar fraction (alkanes), odd-chain length *n*-alkane peaks labeled with carbon chain number.

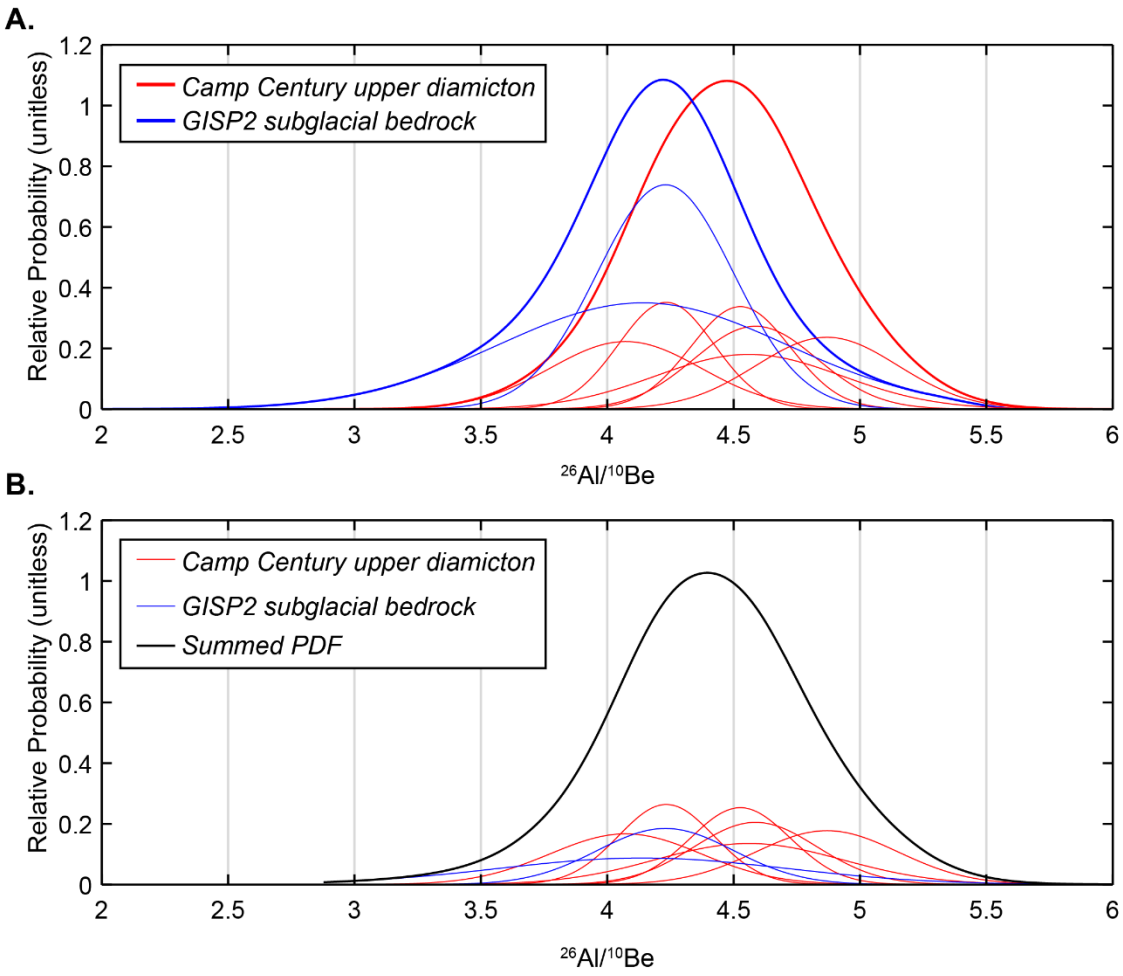

Fig. S9. Comparison of $^{26}Al/^{10}Be$ between Camp Century upper diamicton (red) and GISP2 subglacial bedrock (blue) (13). (A) Thin colored lines kernel density probability functions for individual measurements from each study; thick lines are the summed probability function for each dataset. (B) Similar to above, but the thick black line is the summed probability density function for all samples to demonstrate the agreement between datasets.

Table S1. Pore ice major ions.

Analyte	1059-4		1063-7	
	as measured (mg/L)	corrected for dilution (mg/L)	as measured (mg/L)	corrected for dilution (mg/L)
Ca^{2+}	5.2	13.7	7.4	120.3
Mg^{2+}	2.8	7.3	4.5	73.1
Na^{+}	5.6	14.7	3.4	55.2
K^{+}	0.8	2.1	1.4	22.1
NH_4^{+}	0.00	0.0	0.05	0.8
F^{-}	0.6	1.7	2.0	32.2
Cl^{-}	3.0	7.9	2.0	32.0
NO_3^{-}	0.8	2.2	0.6	10.4
PO_4^{-3}	0.0	0.0	0.0	0.0
SO_4^{-2}	1.0	2.5	1.4	23.5
NO_2^{-}	0.0	0.0	0.0	0.0
Br^{-}	0.2	0.5	0.0	0.0
SiO_2	1.4	3.7	0.5	8.5

Samples aliquots of 3.728 g (1059-4) and 0.491 g (1063-7) were diluted to 9.842 g (1059-4) and 8.017 g (1063-7), giving dilution factors of 2.64 and 16.3, respectively.

Table S2. ^{10}Be Measurements.

					Uncorrected		*Background corrected*[ef]			
Sample Name	**Grain size (μm)**	**Quartz Mass (g)**	**LLNL AMS Cathode Number**	**Mass ^{9}Be Added (μg)**[c]	**^{10}Be/^{9}Be Ratio**[d]	**±1σ**[d]	**^{10}Be/^{9}Be Ratio**	**±1σ**	**[^{10}Be] (atoms g^{-1})**	**±1σ (atoms g^{-1})**
CC1059CF	250-500[a]	26.7889	BE47251	241.5	1.10E-13	3.18E-15	1.10E-13	3.18E-15	6.61E+04	1.92E+03
CC1059CM	500-850[a]	31.1138	BE47252	241.7	1.49E-13	2.47E-15	1.48E-13	2.48E-15	7.69E+04	1.29E+03
CC1059CP	>2000[b]	4.4693	BE48661	186.8	3.00E-14	6.65E-16	2.96E-14	6.72E-16	8.30E+04	2.10E+03
CC1059DF	250-500[a]	16.2598	BE47253	241.9	6.81E-14	1.97E-15	6.73E-14	1.98E-15	6.69E+04	1.97E+03
CC1059DM	500-850[a]	30.6021	BE47255	241.6	1.38E-13	3.05E-15	1.37E-13	3.06E-15	7.22E+04	1.62E+03
CC1059DP	>2000[b]	6.4796	BE48660	187.2	4.67E-14	1.05E-15	4.63E-14	1.05E-15	8.90E+04	2.30E+03
CC1063CF	250-500[a]	14.8130	BE47256	241.3	1.73E-14	7.41E-16	1.66E-14	7.80E-16	1.80E+04	8.49E+02
CC1063CM	500-850[a]	7.5272	BE47257	240.5	8.37E-15	4.88E-16	7.63E-15	5.46E-16	1.63E+04	1.17E+03
CC1063CP	>2000[b]	4.5428	BE48662	187.0	7.33E-15	3.49E-16	6.92E-15	3.62E-16	1.90E+04	1.40E+03

[a] Sample isolated and extracted at the University of Vermont.

[b] Sample isolated and extracted at Lamont-Doherty Earth Observatory, Columbia University.

[c] ^{9}Be was added to samples prepared at UVM through a beryl carrier made at University of Vermont with a concentration of 291 μg mL^{-1}. ^{9}Be was added to samples prepared at LDEO through a beryl carrier made at LDEO with a concentration of 1034.9 μg mL^{-1}.

[d] Isotopic analysis was conducted at LLNL Laboratory; ratios were normalized against standard 07KNSTD3110 with an assumed ratio of 2850 x 10^{-15} (34).

[e] A blank correction of 7.4 ± 2.4E-16 was applied to ^{10}Be/^{9}Be measurements for samples extracted at UVM; see Table S3 for details.

[f] A blank correction of 4.1 ± 1.9E-16 was applied to ^{10}Be/^{9}Be measurements from samples extracted at LDEO; see Table S4 for details.

Table S3. ^{10}Be Blanks (UVM).

Blank Name	UVM Batch Number	LLNL Cathode Number	Be Analysis Date	From AMS: ^{10}Be/^{9}Be Ratio	From AMS: ^{10}Be/^{9}Be Ratio Uncertainty
BLK	662	BE47241	9/19/2019	9.1E-16	1.9E-16
BLKX	662	BE47248	9/19/2019	4.4E-16	1.3E-16
BLK	664	BE47254	9/19/2019	9.6E-16	1.9E-16
BLKX	664	BE47259	9/19/2019	6.4E-16	1.4E-16
			AVERAGE	**7.4E-16**	
			STDEV	**2.4E-16**	

Four blanks were analyzed during this AMS run: 2 from Batch (662) and 2 from batch (664) which were prepared in the same hood, using the same method only 1 week apart. We use the average and standard deviation of the four as the blank correction and uncertainty.

Table S4. ^{10}Be Blanks (LDEO)

Blank Name	LDEO Batch Number	LLNL Cathode Number	Be Analysis Date	From AMS: ^{10}Be/^{9}Be Ratio	From AMS: ^{10}Be/^{9}Be Ratio Uncertainty
BLK1-2020Jun29	2020Jun29	BE48658	7/31/2020	6.5 E-16	1.2E-16
BLK2-2020Jun29	2020Jun29	BE48659	7/31/2020	2.8E-16	8.0E-17
BLK3-2020Jun29	2020Jun29	BE48663	7/31/2020	4.8E-16	1.1E-16
BLK4-2020Jun29	2020Jun29	BE48664	7/31/2020	2.5E-16	7.2E-17
			AVERAGE	4.1E-16	
			STDEV	1.9E-16	

Four blanks were analyzed during this AMS run. We use the average and standard deviation of the four as the blank correction and uncertainty.

Table S5. ^{26}Al measurements

					Uncorrected		*Background corrected*[g,f]			
Sample Name	**Grain size (μm)**	**Quartz Mass (g)**	**PRIME AMS Cathode Number**	**Total ^{27}Al (μg)[c,d]**	**^{26}Al/^{27}Al Ratio[e]**	**±1σ[e]**	**^{26}Al/^{27}Al Ratio**	**±1σ**	**[^{26}Al] (atoms g^{-1})**	**±1σ (atoms g^{-1})**
CC1059CF	250-500[a]	26.7889	159150	3352	1.17E-13	5.74E-15	1.15E-13	5.74E-15	3.22E+05	1.60E+04
CC1059CM	500-850[a]	31.1138	159151	4363	1.06E-13	4.29E-15	1.04E-13	4.30E-15	3.25E+05	1.35E+04
CC1059CP	>2000[b]	4.4693	159396	2054	3.87E-14	2.97E-15	3.77E-14	2.51E-15	3.78E+05	2.91E+04
CC1059DF	250-500[a]	16.2598	159152	1845	1.21E-13	3.82E-15	1.20E-13	3.83E-15	3.03E+05	9.71E+03
CC1059DM	500-850[a]	30.6021	159154	4052	1.14E-13	5.38E-15	1.12E-13	5.39E-15	3.31E+05	1.59E+04
CC1059DP	>2000[b]	6.4796	159395	2143	5.09E-14	3.49E-15	4.99E-14	3.04E-15	3.62E+05	2.49E+04
CC1063CF	250-500[a]	14.8130	159155	1720	1.55E-14	1.20E-15	1.37E-14	1.23E-15	3.55E+04	3.19E+03
CC1063CM	500-850[a]	7.5272	159156	1641	6.60E-15	1.03E-15	4.82E-15	1.07E-15	2.35E+04	5.18E+03
CC1063CP	>2000[b]	4.5428	159397	2105	4.96E-15	1.18E-15	3.99E-15	7.24E-16	3.31E+04	7.87E+03

[a] Sample isolated and extracted at the University of Vermont.

[b] Sample isolated and extracted at Lamont-Doherty Earth Observatory, Columbia University

[c] Samples prepared at UVM: ^{27}Al was quantified by ICP-OES with an internal standard. Based upon quantification of native Al in purified quartz, we added up to 1500 μg of Al using 1000 μg mL-1 SPEX Al standard.

[d] Samples prepared at LDEO: We added LDEO ^{27}Al carrier, made from high purity Al metal with a concentration of 1595 ppm, to samples and blanks, bringing the total ^{27}Al (native + added) to approximately 2 mg for samples and 1.7 mg for blanks, as recommended for the ^{26}Al/^{27}Al analyses at PRIME. Total ^{27}Al (native + added) in each sample was quantified by measuring three splits taken from each of the sample solutions after dissolution, representing 1.3-1.7 % of the total solution. Splits were measured by ICP-OES and calibrated against standards. The spiked blanks with known total ^{27}Al were used as a check of procedural and measurement accuracy.

[e] Isotopic analysis was conducted at PRIME Laboratory; ratios were normalized against standard KNSTD with an assumed ratio of 1.818 x 10^{-12} (2).

[f] A blank correction of 1.8 ± 0.3E-15 was applied to ^{26}Al/^{27}Al measurements for samples extracted at UVM; see Table S6 for details.

[g] A blank correction of 0.98 ± 0.1E-15 was applied to ^{26}Al/^{27}Al measurements for samples extracted at LDEO; see Table S7 for details.

Table S6. ^{26}Al blanks (UVM)

Blank Name	UVM Batch Number	Cathode Number	Al Analysis Date	From AMS: ^{26}Al/^{27}Al Ratio	From AMS: ^{26}Al/^{27}Al Ratio Uncertainty	Number of ^{26}Al Counts
BLK	664	159153	1/13/2020	1.8E-15	5.0E-16	16
BLKX	664	159158	1/13/2020	1.8E-15	4.6E-16	22
			AVERAGE	**1.8E-15**		
			STDEV	**2.0E-17**		
			BLANK UNCERTAINTY [a]	**2.9E-16**		

[a] Blank correction uncertainty calculated using the total number of ^{26}Al counts:

$$Blank\ uncertainty = Avg\ ^{26}Al/^{27}Al\ blank \times \frac{\sqrt{\sum\ ^{26}Al\ counts}}{\sum\ ^{26}Al\ count\ s}$$

Table S7. ^{26}Al blanks (LDEO)

Blank Name	LDEO Batch Number	Cathode Number	Al Analysis Date	From AMS: $^{26}Al/^{27}Al$ Ratio	From AMS: $^{26}Al/^{27}Al$ Ratio Uncertainty	Number of ^{26}Al Counts
BLK2-2020Jun29	2020Jun29	159394	9/2/2020	1.0E-15	4.7E-16	5
BLK3-2020Jun29	2020Jun29	159398	9/2/2020	9.4E-16	4.4E-16	5
			AVERAGE	**9.8E-16**		
			STDEV	**4.9E-17**		
			BLANK UNCERTAINTY [a]	**3.1E-16**		

[a] Blank correction uncertainty calculated using the total number of ^{26}Al counts:

$$Blank\ uncertainty = Avg\ ^{26}Al/^{27}Al\ blank \times \frac{\sqrt{\sum\ ^{26}Al\ counts}}{\sum\ ^{26}Al\ counts}$$

Table S8. $^{26}Al/^{10}Be$ ratios and simple burial ages.

Sample Name	Grain size (μm)	$^{26}Al/^{10}Be$ observed	±1σ	Burial time (myr)[b]	±1σ
CC1059CF	250-500	4.9	0.3	0.9	0.1
CC1059CM	500-850	4.2	0.2	1.2	0.1
CC1059CP	>2000	4.6	0.4	1.0	0.2
CC1059DF	250-500	4.5	0.2	1.0	0.1
CC1059DM	500-850	4.6	0.2	1.0	0.1
CC1059DP	>2000	4.1	0.3	1.2	0.2
	Weighted mean ± σ[a]	**4.5**	**0.3**	**1.0**	**0.1**
CC1063CF	250-500	2.0	0.2	2.8	0.2
CC1063CM	500-850	1.4	0.3	3.5	0.5
CC1063CP	>2000	1.7	0.4	3.1	0.5
	Weighted mean ± σ[a]	**1.8**	**0.4**	**3.2**	**0.4**

[a] Weighted average calculated using the inverse square root of the individual uncertainties for each sample.

[b] Simple burial time calculated using (9) and a $^{26}Al/^{10}Be$ surface production ratio of 7.3±0.3 (6).

Table S9. Luminescence background measurements

Sample Number	Lab ID	Wt % H_20[a]	% K[b]	Rb (ppm)[b]	Th (ppm)[b]	U (ppm)[b]
1059-4	USU-3195	19.4 ± 2.4	1.15 ± 0.03	37.3 ± 1.5	2.76 ± 0.25	1.0 ± 0.10
1063-7	USU-3196	11.7 ± 0.9[c]	1.73 ± 0.04	55.0 ± 2.2	4.89 ± 0.44	0.8 ± 0.10

[a] Sample moisture content based on weight difference following 24 hr in a drying oven.
[b] Elemental content from ICP-AES (K) and ICP-MS (Rb, Th, U), uncertainties based on reported instrumental detection levels
[c] Assumed to have had 20% water content by weight during the duration of burial under the GrIS. Sample interpreted to have dried during storage.

Table S10. Luminescence measurements and ages

Sample Number	Lab ID	Method	Dose Rate[a] (Gy/kyr)	Number of aliquots[b]	Equivalent dose[c], De ± 2se (Gy)	Saturation level[d], 2*Do ± 1σ (Gy)	Apparent IRSL age[e] ± 1se (ka)
1059-4	USU-3195	$IRSL_{50}$[f]	2.28 ± 0.09	4 (4)	>100 ± 30	1150 ± 250	> 45
1063-7	USU-3196	p-$IRSL_{225}$[g]	2.89 ± 0.12	18 (21)	1560 ± 190	1140 ± 620	> 700 ± 70
		MET-p$IRSL_{200, 250}$[h]	2.89 ± 0.12	9 (9)	3590 ± 440	2220 ± 920	> 1350 ± 150

[a] Dose rate calculated from elemental concentrations using conversation factors (22) and corrected for beta-dose attenuation due to grain-size (150-350 μm; (23) and water content (15%; (35)). Dose rates include contribution from internal alpha dose (25) and its attenuation (a-value = 0.089 ± 0.01, (26)). No cosmic contribution to the dose rate due to >1300m of ice cover.

[b] Number of aliquots analyzed and number included in the age calculation within the parentheses. All aliquots were 1-2mm in size, representing 25-50 grains.

[c] Equivalent dose (De) calculated using the central age model (CAM) (21).

[d] The point on which a saturating exponential curve begins to saturate (Do) reflects the maximum De that can be accurately calculated from a sample. De values falling >200% of the Do point may underestimate the true age of a sample.

[e] All infra-red stimulated luminescence (IRSL) age estimates reported here are minimum age estimates due to evidence of light exposure during storage (1059-4) and De values above 200% of saturation (1063-7).

[f] IRSL measurements of potassium feldspar following the single-aliquot regenerative dose procedure for feldspars (16), with measurement at 50°C for 100s following a 250°C preheat for 10s.

[g] IRSL measurements of potassium feldspar followed the high temperature post-infrared IRSL (p-IRSL225, (17, 18) method with IR stimulation at 225ºC for 100s following IR stimulation at 50ºC for 100s and included 3.6%/decade 2-day fading correction (14, 19). Following each regenerative and test dose step, aliquots were preheated at 250°C for 10s to equilibrate unstable components.

[h] IRSL measurements of potassium feldspar followed the multiple elevated temperature p-IRSL method (MET-pIRSL) (20). De values were calculated from p-IRSL signals measured at progressively higher temperatures (50ºC, 100ºC, 150ºC, 200ºC, 250ºC and 300ºC, each measured over 100s). The De values used for age determination were calculated from the 200ºC and 250ºC pIRSL measurement steps (plateau of De results).

Table S11. Water stable isotope chemistry of pore ice.

Sample	$\delta^{18}O$ (‰)	±1σ	δD (‰)	±1σ	Deuterium excess (‰)[a]	±1σ	^{17}O excess (per meg)[b]	±1σ
CC1059	-23.06	0.08	-180.14	0.70	4.3	0.8	35	12
CC1063	-21.49	0.08	-158.53	0.36	13.4	0.4	84	16

Pore ice stable isotope chemistry reported as deviations from VSMOW (Vienna Mean Standard Ocean Water).

[a] Deuterium excess = $\delta D - 8(\delta^{18}O)$

[b] ^{17}O excess = $\ln(\delta^{17}O+1) - 0.528*\ln(\delta^{18}O+1)$

Table S12. Organic geochemistry

Sample	*Analyses at Univ. Washington Isolab*								*Analyses at UVM Stable Isotope Lab*		
	N content (%)	$\delta^{15}N$ vs air N_2 (‰)	±	C content (%)	$\delta^{13}C$ vs VPDB (‰)	±	n	C/N	N content (%)	C content (%)	C/N
1059-4	1.3	2.4	0.8	20.9	-26.7	0.1	2	16.1	0.7	10.6	15.0
1059-4Debris	0.1	-1.1	0.8	2.1	-26.1	0.1	2	21.0	0.5	12.2	23.0
1063-7	0.9	-2.3	0.8	47.7	-29.6	0.1	1	53.0	0.6	29.4	47.4

Table S13. Radiocarbon analysis

UCIAMS #	Sample name	Carbon content (mg C)	Fraction modern	±	$\Delta^{14}C$ (‰)	±	^{14}C age yr BP	±
224017	1059-4 wood	0.0558	0.0085	0.0036	-991.5	3.6	38,300	3400
224018	1059-4 twig	0.32	-0.0004	-0.0005	-1000.4	-0.5	>55,500	

Radiocarbon concentrations are given as fractions of the Modern standard, D14C, and conventional radiocarbon age, following convention (36). Sample preparation backgrounds have been subtracted, based on measurements of ^{14}C-free wood. All results have been corrected for isotopic fractionation according to convention (36), with $\delta^{13}C$ values measured on prepared graphite using the AMS spectrometer. Sample 1059-4 woody tissue yielded a $\Delta^{14}C$ ratio of -991.5±3.6 ‰ with a radiocarbon age equivalent to 38.3±3.4 ^{14}C kyr. Although the 1059-4 wood sample returned a finite age, this sample disintegrated during the solvent sonications and only 56 µg of carbon were available for analysis. The twig result (infinite age on 320 µg of carbon) is considered more reliable.

Table S14. Fatty acid methylated ester (FAME) fraction

Lab ID	Sample Name	Dry Sediment Mass (g)	Mass $C_{20,1}$ added (ng)	Chain-length concentration in sediment (µg/g sed)												
				C20	C21	C22	C23	C24	C25	C26	C27	C28	C29	C30	C31	C32
OC261	1059-4	21.32162	4200	1.20	0.56	2.83	1.12	4.79	0.92	3.17	0.56	2.27	0.31	0.74	0.15	0.25
OC260	1063-7 (2 of 3)	9.14212	4200	0.51	0.27	1.30	0.68	4.07	1.00	4.13	0.75	3.39	0.45	1.04	0.24	0.39
OC262	1063-7 (3 of 3)	21.4012	4200	0.25	0.14	0.62	0.32	1.82	0.46	1.82	0.35	1.51	0.22	0.48	0.13	0.19

Table S15. Alkane Fraction

Lab ID	Sample Name	Dry Sediment Mass (g)	Mass C36 added (ng)	Chain-length concentration in sediment (µg/g sed)												
				C21	C22	C23	C24	C25	C26	C27	C28	C29	C30	C31	C32	C33
OC261	1059-4	9.14212	4600	2.02	4.94	5.69	3.62	5.16	2.23	5.83	1.09	5.55	0.36	5.14	0.02	1.02
OC259	1063-7 (1 of 3)	20.58285	4600	0.34	1.56	0.52	0.78	0.67	0.46	1.23	0.25	1.74	0.20	1.11	0.16	0.20
OC260	1063-7 (2 of 3)	21.32162	4600	0.31	1.08	0.47	0.60	0.50	0.38	0.86	0.27	1.21	0.23	0.84	0.21	0.23
OC262	1063-7 (3 of 3)	21.4012	4600	0.29	1.04	0.43	0.56	0.51	0.34	0.84	0.23	1.13	0.21	0.78	0.17	0.20

Table S16. Camp Century & GISP2 $^{26}Al/^{10}Be$ burial age comparison

	Sample Name	$[^{10}Be]$ (atoms g^{-1})	±1σ (atoms g^{-1})	$[^{26}Al]$ (atoms g^{-1})	±1σ (atoms g^{-1})	$^{26}Al/^{10}Be$	±1σ	Maximum burial duration (myr)[a]	±1σ
Camp Century upper diamicton	CC1059CF	6.6E+04	1.9E+03	3.2E+05	1.6E+04	4.9	0.3	0.9	0.1
	CC1059CM	7.7E+04	1.3E+03	3.3E+05	1.3E+04	4.2	0.2	1.2	0.1
	CC1059CP	8.3E+04	2.1E+03	3.8E+05	2.9E+04	4.6	0.4	1.0	0.2
	CC1059DF	6.7E+04	2.0E+03	3.0E+05	9.7E+03	4.5	0.2	1.0	0.1
	CC1059DM	7.2E+04	1.6E+03	3.3E+05	1.6E+04	4.6	0.2	1.0	0.1
	CC1059DP	8.9E+04	2.3E+03	3.6E+05	2.5E+04	4.1	0.3	1.2	0.2
					Weighted mean ± σ[b]	**4.5**	**0.3**	**1.0**	**0.1**
GISP2 bedrock	GISP2/3/4	2.08E+04	5.20E+02	8.80E+04	5.20E+03	4.2	0.3	1.2	0.1
	GISP 5/6/7	1.33E+04	1.30E+03	5.50E+04	5.40E+03	4.1	0.6	1.2	0.3

[a] For all samples the burial duration is calculated using a $^{26}Al/^{10}Be$ surface production ratio of 7.3 ± 0.3 specific to Greenland (6). For Camp Century samples, we assume production at the surface. The GISP2 samples are measurements in a bedrock core at different depths (13). We show the simple maximum burial duration for comparison with the Camp Century upper diamicton using the same $^{26}Al/^{10}Be$ surface production ratio.

[b] Since the Camp Century analyses consist of different grain sizes across a single depth interval, we show the weighted average using the $^{26}Al/^{10}Be$ uncertainty for each sample as weighting factors. We do not show a weighted average for GISP2 bedrock since it is a depth profile.

SI References

1. J. Fountain, T. M. Usselman, J. Wooden, C. C. Langway, Evidence of the bedrock beneath the Greenland ice sheet near Camp Century, Greenland. *J. Glaciol.* **27**, 193–197 (1981).
2. K. Nishiizumi, Preparation of 26Al AMS standards. *Nucl. Instruments Methods Phys. Res. Sect. B Beam Interact. with Mater. Atoms* **223–224**, 388–392 (2004).
3. G. Korschinek, *et al.*, A new value for the half-life of 10Be by Heavy-Ion Elastic Recoil Detection and liquid scintillation counting. *Nucl. Instruments Methods Phys. Res. Sect. B Beam Interact. with Mater. Atoms* **268**, 187–191 (2010).
4. J. Chmeleff, F. von Blanckenburg, K. Kossert, D. Jakob, Determination of the 10Be half-life by multicollector ICP-MS and liquid scintillation counting. *Nucl. Instruments Methods Phys. Res. Sect. B Beam Interact. with Mater. Atoms* **268**, 192–199 (2010).
5. D. E. Granger, P. F. Muzikar, Dating sediment burial with in situ-produced cosmogenic nuclides: theory, techniques, and limitations. *Earth Planet. Sci. Lett.* **188**, 269–281 (2001).
6. L. B. Corbett, *et al.*, Cosmogenic 26Al/10Be surface production ratio in Greenland. *Geophys. Res. Lett.* **44**, 1350–1359 (2017).
7. G. Balco, J. O. Stone, N. A. Lifton, T. J. Dunai, A complete and easily accessible means of calculating surface exposure ages or erosion rates from 10 Be and 26 Al measurements. **3**, 174–195 (2008).
8. D. E. Granger, J. W. Kirchner, R. C. Finkel, Quaternary downcutting rate of the New River, Virginia, measured from differential decay of cosmogenic 26Al and 10Be in cave-deposited alluvium. *Geology* **25**, 107–110 (1997).
9. P. H. Blard, M. Lupker, M. Rousseau, J. Tesson, Two MATLAB programs for computing paleo-elevations and burial ages from paired-cosmogenic nuclides. *MethodsX* **6**, 1547–1556 (2019).
10. P. H. Blard, M. Lupker, M. Rousseau, Paired-cosmogenic nuclide paleoaltimetry. *Earth Planet. Sci. Lett.* **515**, 271–282 (2019).
11. L. C. P. Martin, *et al.*, The CREp program and the ICE-D production rate calibration database: A fully parameterizable and updated online tool to compute cosmic-ray exposure ages. *Quat. Geochronol.* **38**, 25–49 (2017).
12. G. Balco, Production rate calculations for cosmic-ray-muon-produced 10Be and 26Al benchmarked against geological calibration data. *Quat. Geochronol.* **39**, 150–173 (2017).
13. J. M. Schaefer, *et al.*, Greenland was nearly ice-free for extended periods during the Pleistocene. *Nature* **540**, 252–255 (2016).
14. D. J. Huntley, M. Lamothe, Ubiquity of anomalous fading in K-feldspars and the measurement and correction for it in optical dating. *Can. J. Earth Sci.* **38**, 1093–1106 (2001).
15. D. Banerjee, A. S. Murray, L. Bøtter-Jensen, A. Lang, Equivalent dose estimation using a single aliquot of polymineral fine grains. *Radiat. Meas.* **33**, 73–94 (2001).
16. J. Wallinga, A. Murray, A. Wintle, The single-aliquot regenerative-dose (SAR) protocol applied to coarse-grain feldspar. *Radiat. Meas.* **32**, 529–533 (2000).
17. K. J. Thomsen, A. S. Murray, M. Jain, L. Bøtter-Jensen, Laboratory fading rates of various luminescence signals from feldspar-rich sediment extracts. *Radiat. Meas.* **43**, 1474–1486 (2008).
18. J. P. Buylaert, A. S. Murray, K. J. Thomsen, M. Jain, Testing the potential of an elevated temperature IRSL signal from K-feldspar. *Radiat. Meas.* **44**, 560–565 (2009).
19. M. Auclair, M. Lamothe, S. Huot, Measurement of anomalous fading for feldspar IRSL using SAR. *Radiat. Meas.* **37**, 487–492 (2003).

20. B. Li, Z. Jacobs, R. G. Roberts, S. H. Li, Review and assessment of the potential of post-ir irsl dating methods to circumvent the problem of anomalous fading in feldspar luminescence. *Geochronometria* **41**, 178–201 (2014).

21. R. F. Galbraith, R. G. Roberts, Statistical aspects of equivalent dose and error calculation and display in OSL dating: An overview and some recommendations. *Quat. Geochronol.* **11**, 1–27 (2012).

22. G. Guérin, N. Mercier, G. Adamiec, Dose-rate conversion factors: update. *Anc. TL* **29**, 5–8 (2011).

23. B. J. Brennan, Beta doses to spherical grains. *Radiat. Meas.* **37**, 299–303 (2003).

24. G. Rapp, M. J. Aitken, An Introduction to Optical Dating: The Dating of Quaternary Sediments by the Use of Photon-Simulated Luminescence. *Am. J. Archaeol.* **104**, 129 (2000).

25. V. Mejdahl, Thermoluminescence dating: beta-dose attenuation in quartz grains. *Archaeometry* **21**, 61–72 (1979).

26. J. Rees-Jones, Optical dating of young sediments using fine-grain quartz. *Anc. TL* **13**, 9–14 (1995).

27. J. R. Prescott, J. T. Hutton, Cosmic ray contributions to dose rates for luminescence and ESR dating: Large depths and long-term time variations. *Radiat. Meas.* **23**, 497–500 (1994).

28. M. J. Aitken, J. C. Alldred, The assessment of error limits in thermoluminescent dating. *Archaeometry* **14**, 257–267 (1972).

29. M. . J. Aitken, Thermoluminescent age evaluation and assesment of error limits: revised system. *Archaeometry* **18**, 233–238 (1976).

30. M. J. Aitken, *Thermoluminescence dating*, U.S. ed.. (Academic Press, 1985).

31. T. M. Rittenour, R. J. Goble, M. D. Blum, Development of an OSL chronology for Late Pleistocene channel belts in the lower Mississippi valley, USA. *Quat. Sci. Rev.* **24**, 2539–2554 (2005).

32. A. S. Murray, J. M. Olley, Precision and accuracy in the optically stimulated luminescence dating of sedimentary quartz: A status review. *Geochronometria* **21**, 1–16 (2002).

33. B. M. Vinther, *et al.*, Holocene thinning of the Greenland ice sheet. *Nature* **461**, 385–388 (2009).

34. K. Nishiizumi, *et al.*, Absolute calibration of 10Be AMS standards. *Nucl. Instruments Methods Phys. Res. Sect. B Beam Interact. with Mater. Atoms* **258**, 403–413 (2007).

35. M. J. Aitken, *An introduction to optical dating : the dating of Quaternary sediments by the use of photon-stimulated luminescence* (Oxford University Press, 1998).

36. M. Stuiver, H. A. Pollach, Discussion: reporting of C-14 data. *Radiocarbon* **19**, 355–363 (1977).